ORIENTAL JOURNAL OF CHEMISTRY
An International Open Access, Peer Reviewed Research Journal

www.orientjchem.org

ISSN: 0970-020 X
CODEN: OJCHEG
2026, Vol. 42, No.(1):
Pg.33-42

Highly Efficient and Selective Adsorption of Congo Red and Antibacterial Studies by Para Toulene Sulfonic Acid Functionalized Porous Polypyrrole@MnO$_2$ Nanorods

PRINCE MUFTI ZIAUL HASAN

Center of Nanotechnology, King Abdulaziz University, Jeddah 21589, Saudi Arabia
Correspondence: phasan@kau.edu.sa

http://dx.doi.org/10.13005/ojc/420104

(Received: December 31, 2025; Accepted: February 07, 2026)

ABSTRACT

Herein in situ polymerization was employed to prepare paratoulene sulfonic acid doped polypyrrole (pTSa-Ppy) and polypyrrole@MnO$_2$ (pTSa-Ppy@MnO$_2$). Morphological studies showed MnO$_2$ nanorods embedded inside as well as over Ppy. The X-ray diffraction showed MnO$_2$ and Ppy while the X-ray photon spectroscopy confirmed pTSa doping and showed peaks of Ppy and MnO$_2$. Thus, prepared pTSa-Ppy and pTSa-Ppy@MnO$_2$ were studied for the removal of congo red (CR) and methylene blue (MB) by adsorption. It was found that MnO$_2$, pTSa-Ppy and pTSa-Ppy@MnO$_2$ showed affinity towards CR molecules. The fitting of the Elovich model supported by the highest coefficient of determination i.e. R^2 (0.928) and lowest root mean squared error i.e. RMSE (3.445) indicated that physisorption and chemisorption were involved in bonding between CR and pTSa-Ppy@MnO$_2$.The antibacterial studies against *E. coli* and *B. cereus* showed that control was found to be least effective, with most bacterial growth, followed by pTSa-Ppy and pTSa-Ppy@MnO$_2$.

Key words: adsorption, polypyrrole, morphological analysis, MnO$_2$ nanorods

INTRODUCTION

Industrialization and modernization have resulted in the spills of toxic waste such as dyes, oils, radioactive materials, etc. into the ecosystem[1,2]. It is estimated that over 100 thousand synthetic dyes are in commercial use with over 800 thousand tons of dye production annually worldwide[3]. Textile dyeing is one of the major industrial polluters accountings for over 20% of wastewater generation globally. These highly toxic and non-biodegradable dyes threaten ecosystems by many ways such as: it restricts light penetration into water which affects photosynthesis process, has cytotoxic, neurogenic, teratogenic and carcinogenic effects which leads to skin sensitization, respiratory issues, kidney disorder, liver failure, neurological disturbances, etc[4]. Amongst different dyes, congo red (CR) find a lot of usage in leather, cosmetics, foods, etc. and are discharged into the ecosystem through sewage water. CR due to the above-mentioned adverse properties needs to be efficiently removed for better water quality and economic benefits.

Fortunately, for dye removal, a range of techniques are used such as electro-precipitation, ion exchange, photo-catalysis, reverse osmosis and adsorption. Adsorption is one of the most effective means of dealing with the aforementioned problems associated with the adsorption of dyes because of its feasibility and low cost in preparing the adsorbent for selective adsorption[5]. Conducting polymer-based composites has recently attracted attention as preferred potential adsorbents due to its ease of synthesis and low cost. Mohammad *et al.*[6] reported methyl orange adsorption by Polypyrrole-polyethyleneimine. Similarly, Senguttuvan *et al.*[7] reported that polyaniline-based composite can remove metals and dyes from aqueous systems. Among different conducting polymer polypyrrole (Ppy) has attracted considerable attraction due to its better chemical stability and high yield of synthesis. Apart from polymers, metal oxides have been widely employed as dye adsorbent. Hozefa Dhila *et al.,*[8] showed that metal oxide nanoparticles owing to their functionality and large surface area can enhance the adsorption properties when used as fillers. The report of Patra *et al.*[9] showed that MnO_2 is 98% effective in removing Reactive Blue 21 dye thus making it a highly effective adsorbent. Owing to the exceptional adsorption properties of Ppy and MnO_2 as discussed above, it is believed that the composite of Ppy and MnO_2 can be exploited for adsorptive removal of CR.

Thus, in this work MnO_2 nanorods was prepared via hydrothermal methodology followed by its composite with Ppy and further doping with para toluene sulfonic acid (pTSa). Thus, prepared pTSa-Ppy@$MnO_2$was characterized for structural and morphological characterizations and further exploited for the removal of CR and methylene blue (MB).

EXPERIMENTAL

Materials required

Pyrrole, Ferric chloride, hydrochloric acid (35%) and potassium permanganate were obtained from Sigma Aldrich while p-Toluene sulphonic acid was procured from otto chemicals. For bacterial culture, Nutrient broth media (HiMedia, Mumbai, India), for media and glassware sterilization autoclave (JSAC 80,Daejeon, South Korea), for culture optimum growth incubator (JSGI-150T, Daejeon, South Korea) and calorimeter (Jenway, Stone, Staffordshire, England) and biosafety hood (ESCO, classII BSC,Singapore) was used.

Method

The surface morphology was investigated by field emission scanning electron microscope (FESEM) (model: JEOL, JSM-7600F, FESEM, Tokyo, Japan). X-ray diffraction was done by using monochromatized Al KαX-ray source (α1/4 1486.6 eV) and X-ray photoelectron spectroscopy (XPS) by an ESCALAB 250 from Thermal Fisher Scientific, Warrington, UK.

Dyes removal studies

The selectivity of the fabricated materials was tested on the anionic CR and cationic MB dyes. For this small amount (0.025 g) of material and 25 mL of dye solution were mixed by shaking at 200 rpm. The variation of absorption was studied by varying the solution concentration from 25-200 mg/L, starting from 5 min to 240 min, and pH in the range between 3.0 and 9.0. The UV-visible spectrophotometer was used to analyze the concentrations of the CR and MB at 496 and 665 nm.

Bacterial Strain and Culture Preparation and Treatments

E. coli and *B.cereus* were cultured in nutrient broth under standard aerobic conditions at 37 °C with shaking at 170 rpm. A culture grown for ~12 hours were diluted until an initial optical density (O.D.) of approximately 0.05 before initiating the growth-curve experiment.

Three experimental groups were prepared for both *E. coli* and *B. cereus*. The control cultures did not contain any additional material, which were untreated controls. The second group consisted of cultures treated with pTSa-Ppy of fixed concentration of 100 µg/mL. Third group cultures were exposed to a mixture of pTSa-Ppy@MnO_2 at 100 µg/mL for equal loading across treatments. At the start of incubation, all treatments were introduced without extra supplementation throughout the incubation.

Further, Bacterial growth was monitored by measuring O.D. at 600 nm at variable time intervals over approximately 1000 minutes. Measurements were obtained using a microplate reader, and all experimental groups were analyzed in triplicate. The plotted growth curves represent the mean O.D. values for each condition.

Synthesis of pTSa-Ppy and pTSa-Ppy@MnO_2 composites

For MnO_2 nanorods 1.316 g of $KMnO_4$ and 3 mL of HCl was stirred on magnetic stirrer for 30 minutes. The whole reaction mixture was transferred to Teflon hydrothermal reactor and subsequently heated at 150 ^{0}C for 10 hours. Thus,obtained MnO_2 nanorods was collected and washed by centrifugation, followed by drying at 90 ^{0}C for 10 hours. Ppy was synthesized by insitu oxidative polymerization of pyrrole using $FeCl_3$ as oxidant. In a typical process,0.5 mL of pyrrole was dispersed in 100 mL followed by the addition of oxidant solution $FeCl_3$ (4.67 gm in 100 mL). The whole dispersion slowly turned into black color thereby indicating the formation of Ppy. For the Ppy@MnO_2, 0.05 gm of MnO_2 was added to the pyrrole dispersion 15 minutes after the onset of polymerization and rest separation and washing was done similarly as in the case of MnO_2. Thus, prepared Ppy and Ppy@ MnO_2 was doped with pTSa by dipping in 100 mL of 0.1 M pTSa solution. Finally, pTSa-Ppy and pTSa-Ppy@MnO_2 was removed by centrifugation and subsequently dried at 80 ^{0}C for 12 hours.

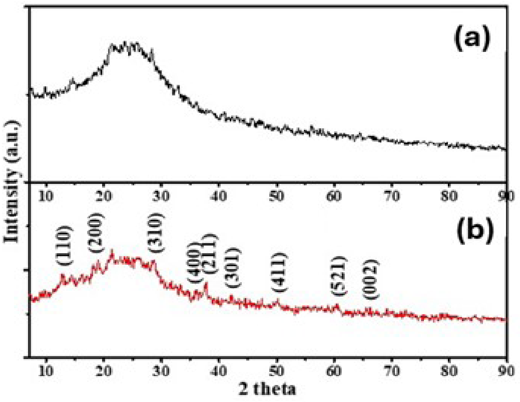

Fig. 1. XRD analysis of pTSa-Ppy (a) pTSa-Ppy@MnO_2 nanocomposite (b).

RESULT AND DISCUSSION

XRD analysis

The XRD of pTSa-Ppy (Fig. 1) shows amorphous broadband at $2\theta=25$ associated with scattering in Ppy chains at interplanar spacings [10,11]. In the case of pTSa-Ppy@MnO_2, apart from the broad $2\theta=25$ peak of Ppy, additional peaks at 12.6, 18.1, 28.6, 37.4, 41.9, 59.9, 60.5 and 64.9 2θ corresponds to (110), (200), (310), (211), (301), (411), (521) and (002) crystal planes of MnO_2 respectively.

XPS analysis

To further elucidate the surface elemental composition of pTSa-Ppy@MnO_2 nanocomposite, XPS analysis was conducted. The survey spectra (Fig. 2) showed the presence of Mn2p and O1s peaks corresponding to the presence of MnO_2 while the C1s and N1s corresponds to the Ppy polymer while S2p corresponds to its successful doping with pTSa.

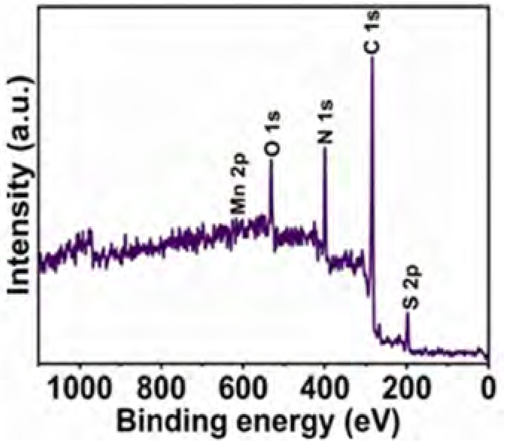

Fig. 2. XPS analysis of pTSa-Ppy@MnO_2 nanocomposite.

Morphology analysis

The morphological analysis of pTSa-Ppy (Fig. 3) shows irregular globular structures of various diameters ~100-400 nm and the globules are interconnected with each other to form long and short chains[14]. In the case of pTSa-Ppy@MnO_2, along with Ppy globules, MnO_2 nanorods can be easily seen embedded as well as on the surface of the polymeric structure[15].

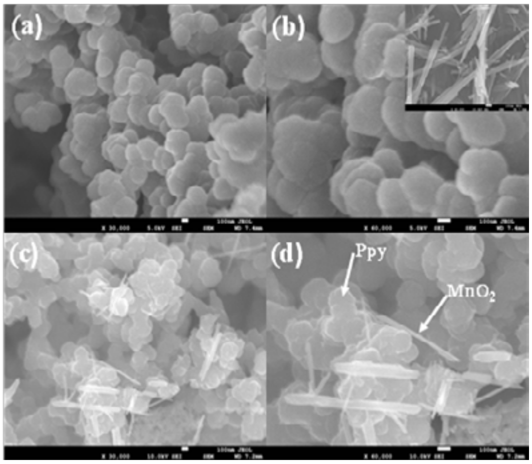

Fig. 3. SEM micrographs of pTSa-Ppy (a,b)and pTSa-Ppy@MnO_2nanocomposite (c,d). Micrograph of MnO_2 nanorods is in inset.

Dyes removal studies

MnO_2, pTSa-Ppy, and pTSa-Ppy@MnO_2 was tested for the decontamination of the CR and MB was tested to determine their selectivity for either anionic or cationic pollutants. From Fig. 4 it can be been that MnO_2, pTSa-Ppy and pTSa-Ppy@MnO_2 have an affinity for the anionic CR molecules. The positively charged amine group on the Ppy enhances adsorption of anionic CR molecules compared to cationic MB [16]. The positive charge in the Ppy and MB repel each other, and electrostatic repulsion was responsible for the lower MB adsorption. Following trend was observed for MB and CR removal: MnO_2<pTSa-Ppy< pTSa-Ppy@MnO_2. This trend indicated that as the functionality of the material increases, the CR scavenging properties of the materials increase. Based on the primary results, CR and pTSa-Ppy@MnO_2 were selected to explore the experimental conditions for optimum adsorption.

Adsorption equilibrium shows the availability of the active sites in the adsorbent. The scavenging of the CR onto pTSa-Ppy@MnO_2 as a function of equilibrium time shows that all the active sites on pTSa-Ppy@MnO_2were fully saturated by CR molecules within 150 min (Fig. 5). The CR interacted with pTSa-Ppy@MnO_2 surface vacant sites quickly within five minutes and process got slower due to the availability of fewer empty sites.

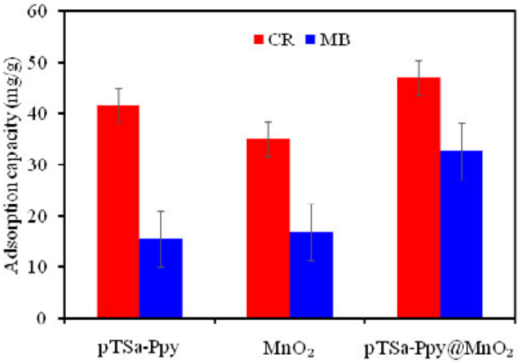

Fig. 4. Plot for the effectiveness testing of the MnO_2, pTSa-Ppy, and pTSa-Ppy@MnO_2 for the decontamination of the anionic CR and cationic MB dyes

The saturation of the pTSa-Ppy@MnO_2 and the rate of the CR scavenging could be analysed by kinetic models by data fitting. Herein, the CR scavenging data was fitted to pseudo-first order, pseudo-second order and Elovich models (Table 1). A non-linear plot for fitting the applied kinetic models is shown in Fig. 5a and the data obtained from their respective equations are included in Table 1. The pseudo-first order shows least fit due to lower R^2 and higher RMSE which means the control of the CR scavenging rate is not subjective to CR distribution over pTSa-Ppy@MnO_2 surface[17]. In contrast the R^2 and RMSE values showed better fit than pseudo-first order but less supportive compared to the Elovich model. Analyzing the results, it was interpreted that mainly chemisorption forces were involved in the CR scavenging onto pTSa-Ppy@MnO_2. The best fitting of the Elovich model is supported by the highest R^2 (0.928) and lowest RMSE (3.445) values demonstrating that physisorption and chemisorption were involved in the bonding between the CR and pTSa-Ppy@MnO_2[18].

The variation in the CR solution pH controls the adsorption process due to the charge in the CR molecular structure and pTSa-Ppy@MnO_2 surface charge. The plot of the CR scavenging onto pTSa-Ppy@MnO_2 at varying solution pH shows that with pH increase from 3 to 9, the CR scavenging reduces. The optimum CR adsorption was recorded at pH 3 (98.1 mg/g) while the lowest result was recorded at pH 9 (78.86 mg/g). The existence of the Hαand αOH in the solution drove the binding of CR onto pTSa-Ppy@MnO$_2$. The presence of the excessive Hαin the solution produces the net positive charge on pTSa-Ppy@MnO$_2$, which facilitates electrostatic bonding forces with anionic CR molecules. The presence of αOH in the solution with CR molecules reduces adsorption as in basic pH conditions due to the repulsive forces between anionic CR as well as deprotonated pTSa-Ppy@MnO$_2$ surface [19]. The results in Fig. 5b indicated that adsorption between pH 3 and 7 varied from 98.1 to 91.69 mg/g, suggesting that pTSa-Ppy@MnO$_2$ is an effective material which can efficiently eliminate the CR dye at a wide pH range[20].

The removal of the CR at various pH can be further explained on functionality on pTSa-Ppy@MnO$_2$. The main constituents of pTSa-Ppy@MnO$_2$ are carbon, nitrogen, oxygen, manganese, and sulfur. The aromatic rings are the main contributor to the binding of CR molecules through the n–n interaction. MnO$_2$ can easily adsorb solution Hαin the acidic solution and have net positive charge (Mn-O + 2HααMn-OHαα), which easily bind with the CR molecules (Mn-OHαα+ CR αMn-OHααCR)[21]. Ppy has the active -NH group which shows the deposition of the Hαin the acidic solution and deprotonation in the basic medium. In acidic medium, protonated amine group binds with the CR molecule through electrostatic interaction while formed H-bond under the basic conditions[22]. Therefore, pTSa-Ppy@MnO$_2$ showed the effective removal of the CR under the acidic and basic medium.

The saturation of the pTSa-Ppy@MnO$_2$

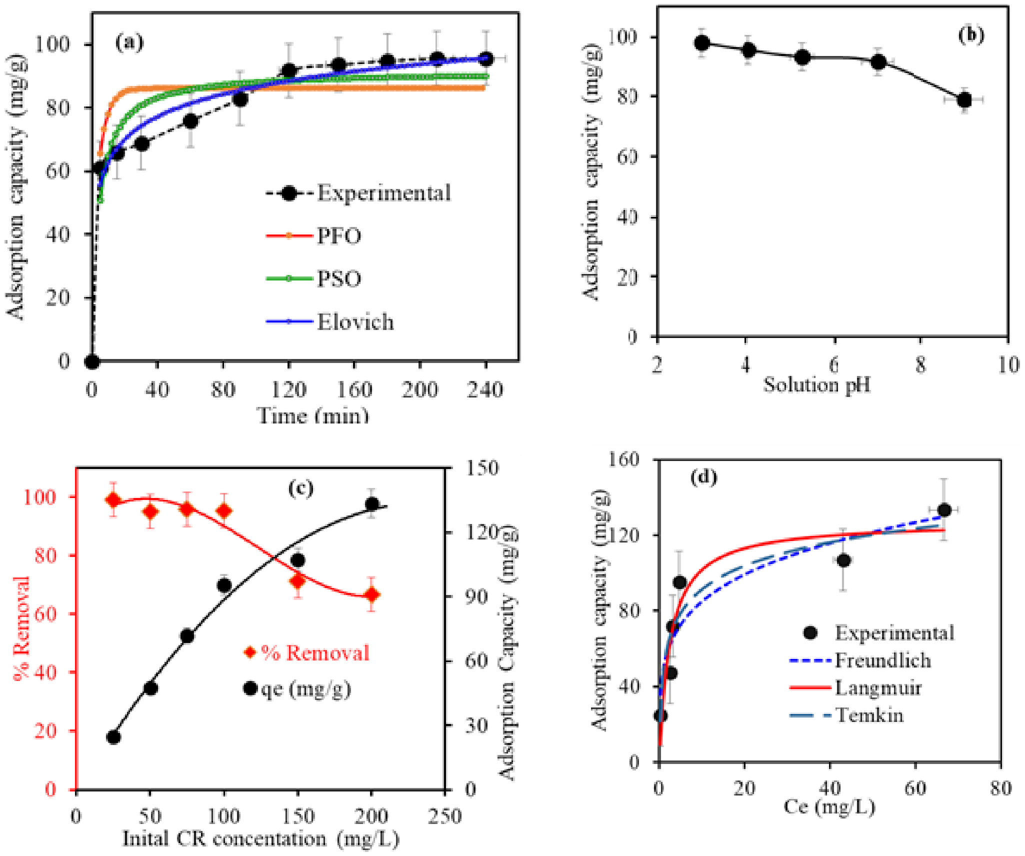

Fig. 5. (a) Plots for the analysis of CR adsorption kinetics onto pTSa-Ppy@MnO$_2$, (b) Influence of the solution pH onto CR scavenging, (c) Removal of the CR at varying initial concentrations, and (d) adsorption isotherm plots for the CR elimination from aqueous solution

Table 1. Kinetics equation and their parameter's values for CR adsorption onto pTSa-Ppy@MnO$_2$

Kinetic model	Parameters	values
Pseudo-first order:		
$q_t = qe\left(1-e^{(-k_1 t)}\right)$	qe (exp.)	95.64 mg/g
	qt (cal.)	86.195 mg/g
	k1	0.194 min−1
	R2	0.374
	RMSE	10.213
Pseudo-second order:		
$q_t = \dfrac{q_e^2 k_2 t}{\left[k_2\left(q_e\right)t+1\right]}$	qe (cal.)	91.614 mg/g
	k2	2.712x10α^{3} mg min−1
	R2	0.684
	RMSE	7.260
Elovich :		
α		459.044 mg/g min−1
$q_t = \dfrac{1}{\beta}\ln\left(\alpha\beta_t\right)$	α	97.927 x10α^{3} g/mg
	R2	0.928
	RMSE	3.445
α		459.044 mg/g min−1
	α	97.927 x10α^{3} g/mg
	R2	0.928
	RMSE	3.445

where: qe(exp.): experimental adsorption capacity; qt(cal.):calculated adsorption capacity k1: pseudo-first order rate constant; R^2:coefficient of determination; RMSE:root-mean-square deviation

active site under the influence of the increasing CR molecules concentrations has been investigated and results are depicted in the Fig. 5c. On increasing the CR concentration from 25 to 200 mg/L, the scavenging capacity of the pTSa-Ppy@MnO$_2$ for CR increases from 24.8 to 133.45 mg/g. This CR adsorption behavior is that rise in CR concentration in the solution augmented the driving force resulting from the concentration gradient, thereby improving CR scavenging. Moreover, a higher initial CR concentration eases a larger rate of collisions between the CR molecules and pTSa-Ppy@MnO$_2$, which resulted in enhanced adsorption capacity[23]. Although, % removal of CR decreased from 99.2 to 66.725%. At lower concentration of 25 mg/L, 99.2% CR removal was recorded owing to excess of active sites available for lower number of CR molecules. These results suggested that as the dye molecules concentration increase, the % removal decreases because active sites on pTSa-Ppy@MnO$_2$ remain constant and become saturated with the rise in CR molecules in the solution[2].

The equilibrium data at the varying concentrations is crucial for understanding the interactions between CR molecules and pTSa-Ppy@MnO$_2$ in equilibrium isotherms. Fig. 5d illustrated the equilibrium adsorption isotherms (Langmuir, Freundlich and Temkin) of CR scavenging onto pTSa-Ppy@MnO$_2$. The calculated parameters of applied isotherm for dye molecules are presented in Table 2. As the calculated constants of isotherms indicated that Temkin model showed highest regression coefficients value and lowest RMSE[25]. These results supports that molecules of CR gets attached though physical as well as chemical forces onto the pTSa-Ppy@MnO$_2$. Moreover, the heterogeneity factor 'n' value (Freundlich constant) for CR scavenging of 4.479 strongly supports the favored adsorption process. These finding indicating

Table 2. Fitted isotherm models values for CR removal by pTSa-Ppy@MnO$_2$

Isotherm model	Parameters	Values 1
Langmuir		
$q_e = \frac{q_m k_L C_e}{1+k_L C_e}$	qm	127. 324 mg/g
	kL	0.399 L/mg
	R2	0.880
	RMSE	12.617
Freundlich		
$q_e = k_F C_e^{\frac{1}{n}}$	n	4.479
	kf	50.881(mg/g)(L/mg)(1/nF)
	R2	0.865
	RMSE	13.378
Temkin		
$q_e = b_T * In\ (K_T * Ce)$	bt	141.3489 J/mol
	kt	16.983 L/mg
	R2	0.910
	RMSE	12.049

where, qm:calculated adsorption capacity; kL:Langmuir constant; R2:coefficient of determination; RMSE:root-mean-square deviation; n:Freundlich constant; kf:Freundlich constant; bt:heat of adsorption; kt:binding constant;

that pTSa-Ppy@MnO$_2$ has the heterogenous surface and CR formed multilayer on material's surface[26,27].

Antibacterial Activity

The growth of *B. cereus* under untreated and treated conditions shows apparent differences in its proliferation in response to pTSa-Ppy and pTSa-Ppy@MnO$_2$. In the control, the *B. cereus* culture showed the most growth overall, showing a clear exponential phase that began within the first 200 minutes. The maximum O.D. reached 1.40–1.45, indicating steady progression of metabolic activity and unimpeded biomass growth.

pTSa-Ppy at 100 µg/mL reduces bacterial growth. The early growth pattern was like that of the control strain, but the exponential phase had a lower slope, and the final O.D. was about 1·05–1·10. This represents a significant attenuation of *B. cereus*, confirming that pTSa-Ppy inhibits cell division and biomass formation moderately and provides strong antimicrobial effects. Among all the cultures, the pTSa-Ppy@MnO$_2$ (total 100 µg/mL) showed the most potent inhibitory effect. The slowest growth rate and the lowest final biomass were recorded in this. Their maximum O.D. values were only 0.95–1.00 and later gradually declined at the end of the measurement (Fig. 6a). The pTSa-Ppy@MnO$_2$ may affect long-term cell integrity or viability as it not only reduces growth but also leads to decline. The increase in efficacy possibly arises from a synergistic interaction between pTSa-Ppy and MnO$_2$. This may happen through generating oxidative stress, disrupting membranes, or targeting critical metabolic processes. The control was found to be least effective, with most bacterial growth, followed by pTSa-Ppy and pTSa-Ppy@MnO$_2$. *B. cereus* is more susceptible to the pTSa-Ppy@MnO$_2$ than to pure pTSa-Ppy, providing evidence that integrating MnO$_2$α nanoparticles enhances the antibacterial properties of the polymeric system significantly. These results show that pTSa-Ppy@MnO$_2$ composites can be effective antimicrobial agents, especially against Gram-positive bacteria such as *B. cereus*.

The growth curves show that the impact of pTSa-Ppy and pTSa-Ppy@MnO$_2$ on *E. coli* over the monitored period does not change much. The growth of control untreated *E. coli* were sharply exponential after about 200 min, reaching a stationary-phase

O.D. of 0.95–0.98, indicating normal, unhindered bacterial growth. In contrast, treatment with 100 µg/mL of pTSa-Ppy reduced bacterial growth. The culture followed a similar initial lag and early exponential phase as the control in Fig. 6b. However, the overall slope during the exponential phase was lower, and the final O.D. was approximately 0.67, indicating moderate growth inhibition by pTSa-Ppy. The reaction did not completely inhibit bacterial growth, but it affected the *E. coli* metabolic activity and cell division.

The culture treated with pTSa-Ppy@MnO_2 (total: 100 µg/mL) shows the highest inhibitory action. This group grew more slowly than exponentially. Biomass was not growing as fast as in the case of control or pTSa-Ppy@MnO_2. The culture reached an O.D. of approximately 0.55. However, this reading then began to slightly decrease towards the end of the measurement period. This suggests two things: first, that growth was inhibited; and second, that there may have been destabilization or a partial loss of viability after prolonged exposure. This shows that the combination of pTSa-Ppy and MnO_2 has a synergistic effect against microbes. pTSa-Ppy works better with MnO_2 nanoparticles, possibly by increasing oxidative stress or by promoting interactions across the bacterial membrane.

The growth curve analysis demonstrated that both *E. coli* and *B. cereus* reacted differently to pure pTSa-Ppy and pTSa-Ppy@MnO_2. *B. cereus* has demonstrated superior biomass production when compared to *E. coli* under all conditions. In control conditions without treatment both bacteria grew at a relatively consistent rate and also displayed free metabolic activity. When treated with pure pTSa-Ppy at 100 µg/mL, both species were moderately inhibited, although *E. coli* experienced a greater inhibitory effect while *B. cereus* tolerated Ppy more effectively. In *E. coli*, the pTSa-Ppy@MnO_2 at a total dose of 100 g/mL shows the most potent antimicrobial activity, reducing the final O.D. values to ~0.55. and ~0.95–1.00 in *B. cereus*. Both species exhibited slight declines in O.D. at later time points, suggesting growth inhibition and possible destabilization or partial loss of viability with prolonged exposure. Comparatively, *E. coli* was more sensitive to both pTSa-Ppy and pTSa-Ppy@MnO_2 than *B. cereus*. Despite this, the same hierarchical trend was observed in this organism: Control >pTSa-Ppy>pTSa-Ppy@MnO_2, indicating that MnO_2 nanoparticles enhanced antimicrobial activity. The research conducted showed that the combination of $MnO_2\alpha$ and Ppy has superior antimicrobial activity. In addition, it was found that *E. coli* was more susceptible than *B. cereus*.

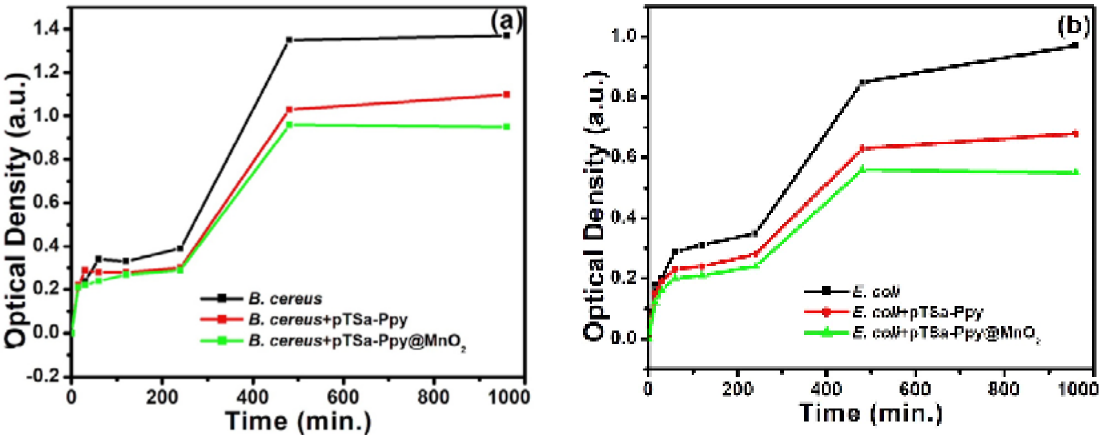

Fig.6. (a) The bacterial growth kinetics of *B. cereus* and (b) *E.coli* in the absence and presence of pTSa-Ppy and pTSa-Ppy@MnO_2nanocomposite.

CONCLUSION

In summary, this work demonstrates that MnO_2 insertion and doping with paratoulene sulfonic acid of Ppy improves the selective adsorption of anionic CR dye. The morphological analysis showed the features of both MnO_2 nanorods and porous Ppy structures. The structural analysis by XRD and XPS showed that MnO_2 is well interacted with Ppy and its successful doping with pTSa. The pTSa-Ppy and pTSa-Ppy@MnO_2 showed selective adsorption of anionic CR in contrast to cationic MB dye which was poorly adsorbed. The highest R^2 of 0.928 and lowest RMSE of 3.445 suggested that adsorption was predominated by the physisorption as well as chemisorption forces.The antibacterial studies against *E. coli* and *B. cereus* showed that the control was found to be least effective, with most bacterial growth, followed by pTSa-Ppy and pTSa-Ppy@MnO_2. These results show that pTSa-Ppy@MnO_2 composites can be effective antimicrobial agents against Gram-positive and Gram-negative bacteria.

ACKNOWLEDGMENTS

The author, P.M.Z. Hasan is grateful to the Centre of Nanotechnology, King Abdulaziz University for providing the research facilities.

REFRENCES

1. Fendi W.J.; Naser, J.A. *Orient. J. Chem.* **2018**,34 (6). http://dx.doi.org/10.13005/ojc/340628
2. Raj, A.K., Orient. J. Chem. **2025**, 41(2), http://dx.doi.org/10.13005/ojc/410236
3. Yadav, S.; Jilani, A.; Sachan, S.; Kumar, P.; Ansari, S.A.; Afzal, M.; Ansari, M.O. *Chemistry.*,**2024**, 6(3), 489. https://doi.org/10.3390/chemistry6030028
4. Kumar, R.; Ansari, M.O.; Parveen, N.; Barakat, M.A.; Cho, M.H. *RSC Adv.* **2015**, 5, 61486. https://doi.org/10.1039/C5RA10378A
5. Ansari, M.O.; Kumar, R.; Parveen, N.; Barakat, M.A.; Cho, M.H.,NJC, *New J. Chem.* **2015**, 39, 7004. https://doi.org/10.1039/C5NJ01443C
6. Mohamad, N.; Salleh, N.M.; Mahmud, H.N.M.E., *J. Polym. Mater.* **2024**,40, 165. https://doi.org/10.32381/JPM.2023.40.3-4.4
7. Senguttuvan, S.; Senthilkumar, P.; Janaki, V.; Kamala-Kannan, S., *Chemosphere.* **2021**, 267, 129201. https://doi.org/10.1016/j.chemosphere.2020.129201
8. Dhila, H.;Bhapkar, A.; Bhame, S., *Desalin Water Treat.* **2025**,321, 101004. https://doi.org/10.1016/j.dwt.2025.101004
9. Patra, T.; Mohanty, A.; Singh, L.; Muduli, S.;Parhi, P.K.;Sahoo, T.R., *Chemosphere.* **2022**, 288, 132472.https://doi.org/10.1016/j.chemosphere.2021.132472
10. Iqbal, J.; Numan, A.; Ansari, M.O.; Jagadish, P.R.; Jafer, R.; Bashir, S.; Mohamad, S.; Ramesh, K.; Ramesh, S.,Electrochim. Acta. **2020**,348, 136313.https://doi.org/10.1016/j.electacta.2020.136313
11. Jafer, R.;Alsufyani, S.A.;Iqbal, J.;Ansari, M.O.;Numan, A.;Bashir, S.;Hasan, P.M.Z.; Wageh, S., *Polymers*. **2023** 15(5), 1267. https://doi.org/10.3390/polym15051267
12. Iqbal, J.; Ansari, M.O.; Numan, A.;Wageh, S.;Al-Ghamdi, A.; Alam, M.G.; Kumar, P.; Jafer, R.; Bashir, S.;Rajpar, A.H., *Polymers*. **2020**, 12(12):2918. 10.3390/polym12122918
13. Ansari, S.A.; Parveen, N.; Han, T.H.; Ansari, M.O.; Cho, M.H., *Phys. Chem. Chem. Phys.* **2016**,18, 9053. https://doi.org/10.1039/C6CP00159A
14. Yuan, X.; Li, L.; Ma, Z.; Yu, X.; Wen, X.; Zi-Feng Ma; Zhang, L.; Wilkinson, D.P.; Zhang, J., *Scientific Reports*. **2016**, 6, 20005. https://doi.org/10.1038/srep20005
15. Farrokhi, H.; Khani, O.; Nemati, F.;Jazirehpour, M., *Synth. Met.* **2016**, 215, 142.https://doi.org/10.1016/j.synthmet.2016.02.016
16. Ansari, M.O.; Kumar, R.; Ansari, S.A.; Ansari, S.P.;Barakat, M.A.;Alshahrie, A.; Cho, *J. Colloid Interface Sci.* **2017**, 496, 407. https://doi.org/10.1016/j.jcis.2017.02.034
17. Wang, T.; Jiang, M.;Yu, X.;Niu, N.; Chen, L., *Sep. Purif. Technol.* **2022**, 302, 122116. https://doi.org/10.1016/j.seppur.2022.122116
18. Gamboa, D.M.P.;Abatal, M.; Lima, E.; Franseschi, F.A.;Ucán, C.A.; Tariq, R.; Elías, M.A.R.; Vargas, J., *Int. J. Mol. Sci.* **2024**, 25(9), 4771. https://doi.org/10.3390/ijms25094771
19. Mousavi, S.H.; Yaghoobi, M.;Asjadi, F., *Sci. Rep.* **2024**, 14, 18505 (2024); https://doi.org/10.1038/s41598-024-69432-1
20. Ali, H.; Ismail, A.M., *J. Polym. Environ.* **2022**, 31, 976. https://doi.org/10.1007/s10924-022-02663-3
21. Yang, Q.; Song, H.; Li, Y.; Pan, Z.;Dong, M.;

Chen, F.; Chen, Z.,*J. Mol. Liq.*__2017__, 234, 18. https://doi.org/10.1016/j.molliq.2017.03.028

22. Aigbe, U.O.;Khenfouch, M.; Ho, W.H.; Maity, A.;Vallabhapurapu, V.S.;Hemmaragala, N.M.,*Desalin. Water. Treat*. **2018**, 131, 328 (2018);https://doi.org/10.5004/dwt.2018.23028
23. Bounaas, M.;Bouguettoucha, A,;Chebli, D.; Derbal, K.; Benalia, A.; Pizzi, A.,*Appl. Sci.* **2024**, 14(22), 10365. https://doi.org/10.3390/app142210365
24. Gupta, V.K.; Kumar, R.; Nayak, A.; Saleh, T.A.; Barakat, M.A.,*Adv. Colloid. Interface Sci*. **2013**, 193, 24.https://doi.org/10.1016/j.cis.2013.03.003
25. Firmino, H.C.T.; Nascimento, E.P.; Costa,K .C.;Arzuza,L.C.C.;Araujo,R.N.; Sousa,B.V.; Neves,G.A.; Morales,M.A.; Menezes, R.R.,*Materials*. 2025,18(4), 754.https://doi.org/10.3390/ma18040754
26. Ige.A.O.;Ogunsile,B.O.; Ore,O.T.; Olawade,D.B.,*Discov. Chem*. **2024**, 1, 9. https://doi.org/10.1007/s44371-024-00010-0
27. Boahen, G.O.; Sewu, D.D.; Tran,H. N.; Woo, S. H.,*Colloids and Surfaces A: Physicochemical and Engineering Aspects*. **2021**, 625, 126911. https://doi.org/10.1016/j.colsurfa.2021.126911